Proceedings of
11th European Conference on Turbomachinery Fluid dynamics & Thermodynamics
ETC11, March 23-27, 2015, Madrid, Spain

COMPARISON OF DIFFERENT METHODS FOR THE ANALYSIS OF TIME-RESOLVED FLOW FIELD MEASUREMENTS IN AN AXIAL TURBINE

T. Kluge – M. Henke – J. R. Seume

Institute for Turbomachinery and Fluid Dynamics - TFD
Leibniz Universität Hannover
Appelstraße 9, 30167 Hannover, Germany
kluge@tfd.uni-hannover.de

ABSTRACT

To resolve secondary flows and wakes in turbomachinery measurements, reduction methods capable of isolating the deterministic and stochastic components of a given signal must be implemented. In the present study, two approaches are applied: a trigger-based phase-locked ensemble averaging technique and a newly proposed method based on the deconvolution of the signal in the frequency domain. While the former is used in numerous publications on the measurement of secondary flows, the latter has – to these authors' knowledge – not yet been used in this context. Both data reduction techniques are outlined theoretically and applied to unsteady pressure measurements in a multi-stage axial turbine. Results obtained from the proposed deconvolution method are in good qualitative agreement with ensemble-averaged data. In some cases, a quantitative discrepancy is shown, most likely caused by numerical errors. Nevertheless, within certain boundaries the method is capable of isolating the deterministic signal including non-rotationally harmonic components without the need for a trigger signal.

NOMENCLATURE

f	frequency	$\widetilde{p}$	periodically fluctuating signal component
G	generic signal spectrum	p'	stochastically fluctuating signal component
g	generic signal components	T	characteristic period
K	number of ensemble traces	thr	threshold
P	signal spectrum	x	threshold value
p	(pressure) signal	γ	gain factor
$\overline{p}$	constant signal component	φ	phase

INTRODUCTION

Unsteady Flow in Turbomachinery

Over the last few years, the design process of turbomachinery components such as multi-stage axial compressors and turbines has changed. While previously the design focused on the time averaged steady-state flow field and design point operation of the compressor or turbine, new and more powerful numerical methods made it possible to account specifically for unsteady flow effects and off-design operation during the design process as well. This development has also been driven by the requirements of the market, as modern gas turbines must be able to operate at part- and low-load conditions while maintaining a high level of efficiency. Thus, the unsteady investigations of the flow field as conducted by several authors (Meyer, 1958; Niehuis *et al.*, 1990; Restemeier, 2012) and described in a more general approach by Mailach (2010) needs to be validated by further measurements in order to prove the ability of numerical methods to predict the unsteady flow correctly.

Simultaneously, the development of unsteady measurement techniques allows the recording of larger amounts of unsteady flow data in increasingly complex test set-ups. In order to obtain and analyse

as much information as possible from unsteady measurements, and to reduce the data collected in a way they can be handled more easily, several methods of data processing and data reduction can be applied to the raw signals in order to account for the characteristics of different flow phenomena. Methods to analyse the recorded signals mainly focus on harmonically periodic effects such as the wakes of rotating blades (Gostelow, 1977). However, a number of non-harmonically occurring unsteady effects like rotating stall in compressors and rotating instabilities due to windage in turbines under low load conditions (Binner and Seume, 2014) can be investigated using different data analysis techniques.

Time-Resolved Probe Measurements

As noted by many authors (e.g. Sieverding, 1985; Sharma *et al.*, 1985; Mailach *et al.*, 2004), the flow in turbomachinery is highly unsteady, viscous and three-dimensional. Mailach *et al.* concludes that the main source of unsteadiness in turbomachinery is the aerodynamic interaction between rotor and stator blades. These unsteady effects are even more pronounced in conjunction with transonic blade designs, as shock waves develop in the blade passage and near the trailing edge of the blades, leading to an increasing unsteady interaction between blade rows (Bräunling, 2009; Rick, 2013). In addition to the periodically alternating incidence angle at the blade leading edge, which causes an unsteady pressure distribution on the profile itself, blade profile losses can also change due to transition effects triggered by the unsteady flow influencing the profile boundary layer (Schlichting and Gersten, 2006). Thus, the detailed knowledge of the behaviour and the development of the unsteady flow between rotating blade rows is of great importance. Although, several measurement techniques like hot-wire anemometry and different optical measurement methods have been developed and applied to the measurement of the unsteady velocity distribution, the measurement of unsteady pressure distribution using fast response pressure probes is a well suited method to obtain information about the unsteady flow field between blade rows. In many cases, the magnitude of the unsteady components of the flow field is fairly small compared to the predominant steady components. This fact leads to a critical signal-to-noise ratio in real applications, necessitating the application of different kinds of filters and data reduction methods to the raw signal, as described below.

EXPERIMENTAL TEST SETUP

TFD Model Air Turbine Test Rig

The model air turbine test rig at the *Institute of Turbomachinery and Fluid-Dynamics* (TFD) is used to collect the experimental data for the present work. The test rig consists of a turbine section with a conventional steam turbine split-casing design, making it possible to install different types of turbine configurations by changing the inner components like the rotor and the vane carrier.

The compressed air is provided by three screw compressors with a maximum mass flow rate of $9.2\,{}^{kg}/_{s}$ and a maximum pressure ratio of 3.3. An automatic controller stabilising the operating point of the turbine is used. Thus, it is possible to attain good operating point stability for measurements such as complex steady as well as unsteady probe traverses. This leads to only small measurement errors due to environmental changes of the measurement point and, thus the experimentally obtained data can be considered reliable. Table 1 and 2 show an overview of the test rig's maximum operating parameters and characteristics.

The power generated by the turbine is dissipated using an electric direct current (DC) machine, serving as a generator or motor, if needed. The DC-machine permits the independent adjustment of turbine output power from the rotational speed. The rotational speed is measured by a torque meter device as well as by a toothed wheel, providing a rotor-based trigger signal for unsteady flow measurements. The mass flow is measured by a Venturi nozzle located upstream of the turbine inlet, which has been calibrated at Deutscher Kalibrierdienst (DKD). Thermal effects are accounted for by correcting the nozzle diameter for the temperature. As the blading section of the turbine has

Table 1: **Maximum operating conditions and inlet parameters of the model air turbine test rig**

Test rig parameters		**accuracy**	**stability**
max. rotational speed n	7500 rpm	± 1 rpm	± 12 rpm
max. mass flow rate $\dot{m}$	9.2 kg/s	$\pm 0.18\,\%$	$\pm 0.53\,\%$
max. inlet temperature T_{in}	450 K	± 0.4 K	± 0.8 K
inlet turbulence Tu	$1.2 \ldots 2\,\%$		
max. power output	1300 kW		

Table 2: **Turbine model specific parameters**

Turbine parameters	
avg. hub/shroud ratio	0.55
number of stages	7
max. inlet-to-outlet pressure ratio Π	3.3
max. inlet total pressure $p_{tot,in}$	3.5 bar

an axial length of up to 1.1 m, up to seven turbine stages can be installed on the rotor. During the measurements conducted for this study, the test rig was equipped with a seven stage high-pressure steam turbine blading as shown in Fig. 1. Numerous experimental and numerical studies on this blading have been conducted (Herzog *et al.*, 2007). Additional information about the blading and experimental results of part- and low load condition measurements can be found in Binner and Seume (2014) and Binner (2011).

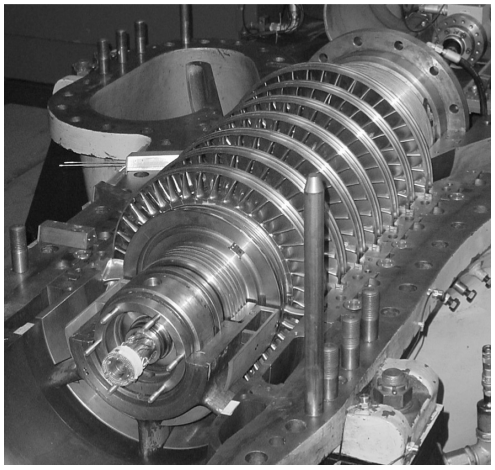

Figure 1: **7-stage turbine rotor and test rig (Binner and Seume, 2014)**

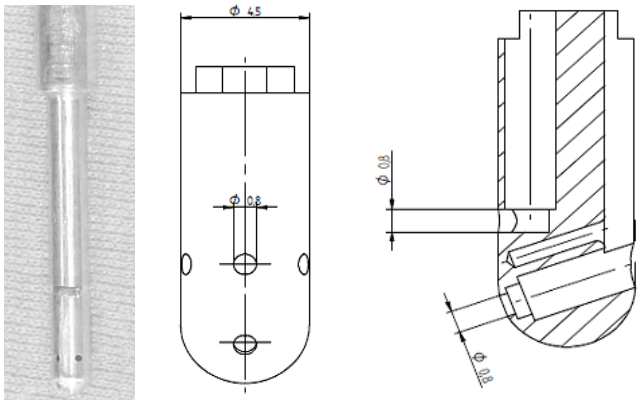

Figure 2: **Four-hole probe ZI45 for unsteady flow measurements (all dimensions in mm) (Rieß and Braun, 2003)**

Unsteady pressure probe ZI45

The unsteady multi-hole pressure probe ZI45 that was developed, tested, and calibrated at the TFD by Rieß and Braun (2003) was used to conduct the measurements for the present study. The ZI45 probe uses a cylindrical probe head geometry with a diameter of 4.5 mm. The probe is designed as a 4-hole probe in order to obtain the unsteady three-dimensional flow vector. Cylindrical piezo-resistive pressure transducers Kulite XCS-062 are used within the probe. The resonance frequency (18 to 25 kHz) is well above the blade passing frequency of the measurement data presented below. Figure 2 shows the overall dimensions of the probe head section. Further information about the probe and the calibration process can be found in Rieß and Braun (2003) and Bubolz (2005). The measurement uncertainty of the probe (approximately ± 1.82 mbar) is at least an order of magnitude smaller than the deterministic fluctuations analysed in this study.

DATA REDUCTION METHODS

The raw time-resolved pressure traces (or any other time-resolved signal recorded by an appropriate measurement device)

$$p(t) = \overline{p} + \widetilde{p}(t) + p'(t) \tag{1}$$

are defined as a superposition of three separate components: (1) a constant component, (2) a periodically fluctuating component, and (3) a stochastically fluctuating component. The aim of the following data reduction methods is to isolate the deterministic signal $p_{\mathrm{det}}(t) = \overline{p} + \widetilde{p}(t)$. As such, the methods are intended primarily for the reduction of unsteady measurement data and analysis of the secondary flow structures therein. The data are not used to compute performance parameters, mass flow or other derived quantities. The main advantage of the deconvolution method is its postulated ability to reconstruct non-rotationally harmonic signal components.

Phase-Locked Ensemble Average

The *phase-locked ensemble average* (PLEA) as proposed by Gostelow (1977) is a well-known and widely used method for the reduction of strongly periodic data. If the periodic fluctuation can be regarded as stationary, ensemble averaging a number of K traces (each the duration of a multiple of the characteristic period) will eliminate the stochastic component while preserving the deterministic signal. It is crucial to ensure that individual ensemble members are in phase before averaging.

In practical terms, if a time-resolved pressure signal and a synchronous trigger signal (e.g. one short rectangular pulse per revolution) are recorded, the pressure signal can be cut into traces corresponding to one revolution of the turbine. Depending on the stability of the rotational speed, the traces will contain varying numbers of discrete measurements. In that case, phase-locking can be achieved by simple linear or *nearest neighbour* interpolation on a common grid.

The PLEA is computed according to

$$p_{\mathrm{det}}(t) = \lim_{K\to\infty} \frac{1}{K} \sum_{k=1}^{K} p\left(t + kT\right) = \overline{p} + \lim_{K\to\infty} \frac{1}{K} \sum_{k=1}^{K} \left[\widetilde{p}\left(t + kT\right) + p'\left(t + kT\right)\right] \tag{2}$$

$$\because \lim_{K\to\infty} \frac{1}{K} \sum_{k=1}^{K} p'\left(t + kT\right) \to 0\,, \tag{3}$$

where T is a multiple of the characteristic period (e.g. corresponding to one revolution of the turbine shaft). While the size of the ensemble, K, necessary to achieve satisfactory results depends on the signal-to-noise ratio, it has been found that averaging 300 to 500 traces (i.e. revolutions) is sufficient for the data used in this paper. Other authors have deemed ensembles of 100 (Ristic *et al.*, 1999) or even 50 traces (Restemeier, 2012) adequate, though 232 traces were used in the latter study.

The stochastic component is readily found by subtracting the deterministic component from the phase-locked raw data traces

$$p'_{\mathrm{k}} = p'(t + kT) = p(t + kT) - p_{\mathrm{det}}(t) \tag{4}$$

containing signal noise as well as measured fluctuations, e.g. turbulence.

The main drawback of the PLEA method is its limitation to the recovery of those periodic components of the signal whose frequency is a (sub-)multiple of the characteristic frequency, e.g. the rotational frequency. The deconvolution method proposed in the following section is an attempt to resolve this problem.

Deconvolution

A method proposed by Camp and Shin (1995) and augmented by Lengani *et al.* (2012) can be used to analyse the stochastic components of a given signal: After using the Fast-Fourier-Method to transform the signal in the frequency domain, all (sub-)multiples of the rotational frequency are set to zero as well as other distinctly periodic components (Lengani *et al.*, 2012). The remaining "chopped" spectrum may then be inversely Fourier-transformed or used to compute the integral turbulent length scale via the autocorrelation function.

Algorithm

The deconvolution method proposed here is based on that approach as well as the CLEAN algorithm first introduced by Högbom (1974) to achieve the opposite, i.e. the recovery of the periodic signal component and, thus, posing an alternative to the PLEA without the need for a trigger signal. Instead of eliminating the periodic components of the signal spectrum after transformation in the frequency domain, they are extracted in an iterative process to assemble the deterministic signal. The algorithm (cf. Fig. 3) implements the following steps:

1. Computation of the complex spectrum $\mathrm{P(f)} = \mathcal{F}(\mathrm{p})(\mathrm{t})$ by Fourier transformation
2. Definition of a threshold value $\mathrm{P_{thr}}$ serving as abort criterion of the iteration loop
3. Computation of the absolute-valued spectrum $\mathrm{P_{abs}(f)} = |\mathrm{P(f)}|$
4. Identification of the frequency $\mathrm{f_{max}}$ of the maximum amplitude $\mathrm{P_{max}} = \max\left(\mathrm{P_{abs}(f)}\right)$ as well as the corresponding phase $\varphi_{\max}$
5. Multiplication of the maximum Amplitude $\mathrm{P_{max}}$ and a pre-defined loop gain γ $(0 < \mathrm{gain} \leq 1)$
6. Formation of a generic cosine signal $\mathrm{g_i(t)}$ of the same length as the original noisy signal, amplitude $\gamma \mathrm{P_{max}}$, and Phase $\varphi_{\max}$, where i denotes the loop counter
7. Fourier-Transformation of the generic signal $\mathrm{G_i(f)} = \mathcal{F}\left(\mathrm{g_i}\right)\left(\mathrm{t}\right)$
8. Subtraction of the spectra $\mathrm{P'_{abs}(f)} = \mathrm{P_{abs}(f)} - \mathrm{G_i(f)}$ while eliminating negative values by setting them to 0
9. Iteration by defining $\mathrm{P_{abs}} \coloneqq \mathrm{P'_{abs}}$ and continuing with item 3, while the maximum of $\mathrm{P'_{abs}}$ is less than the threshold value defined above
10. Computation of $\mathrm{p_{det}} = \sum_{\mathrm{i}} \mathrm{g_i(t)}$ if $\max\left(\mathrm{P'_{max}(f)}\right) < \mathrm{P_{thr}}$

Ideally, the remaining spectrum would contain the intermittent signal components with artefacts due to the leakage-effect of periodic component frequencies eliminated. Depending on the choice of the threshold value, the reassembled signal contains all deterministic periodic components of the raw signal including the constant component. Provided all periodic component frequencies of the recorded signal are a (sub-)multiple of the characteristic frequency, the deconvolved signal is equivalent to the ensemble-averaged signal. A comparison of both methods, based on a generic signal, is made in the following section.

The iterative process in the frequency domain is illustrated in Fig. 4. The initial absolute-valued spectrum $P_{abs}(f)$ of a generic signal (cf. Fig. 5) is plotted in the uppermost graph, the largest signal component being the constant pressure at 0 Hz which, due to the logarithmic scale, is not visible. There are several periodic components above the dashed threshold, but there are also some spurious components. These are not actually periodic components but side lobes resulting from the FFT window function. When the constant component is processed during the first (or the first few) iterations,

these side lobes (and those of other signal components) are removed (item 8), hence the iterative process. Gradually, all periodic components above the threshold value are processed and the "clean" signal is compiled.

Noise of the same frequency as each of the periodic signal components contributes to the amplitude of the initial signal spectrum. To ensure that no signal component below the threshold value is processed, the loop gain would have to be infinitesimal (Högbom, 1974). This however is not practical so that a value of $\gamma = 0.3 \ldots 1$ is chosen. If the gain factor is chosen to be unity, erroneous components contained in the signal at the periodic frequencies, i.e. noise or side lobes resulting from the FFT, are processed as part of the deterministic signal and contribute to its amplitude.

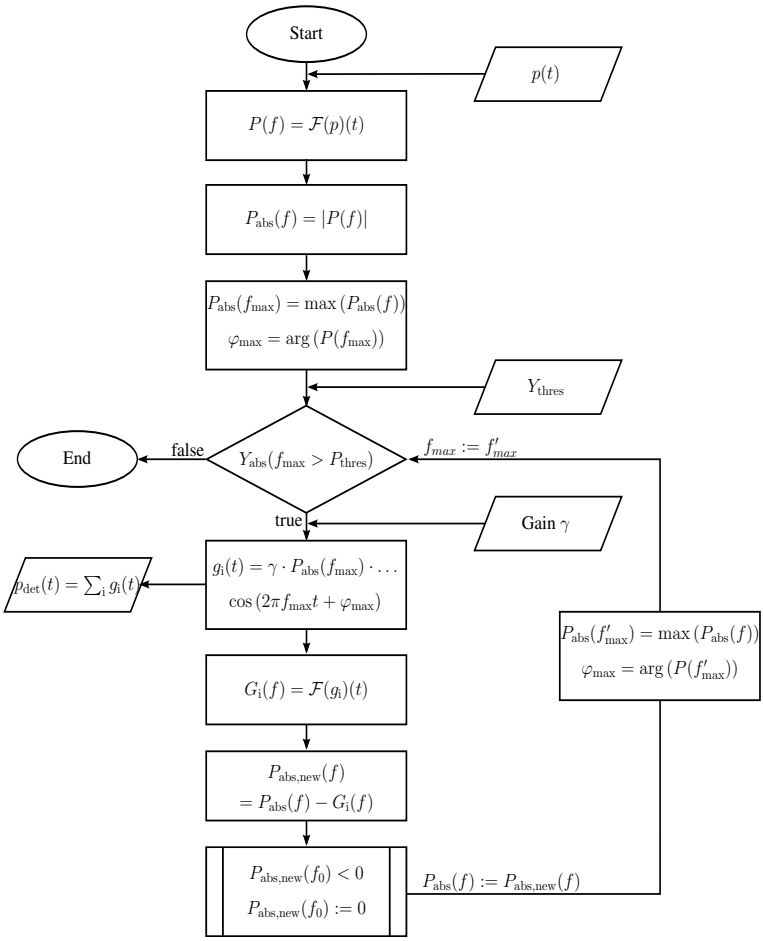

Figure 3: **Flowchart of the deconvolution algorithm**

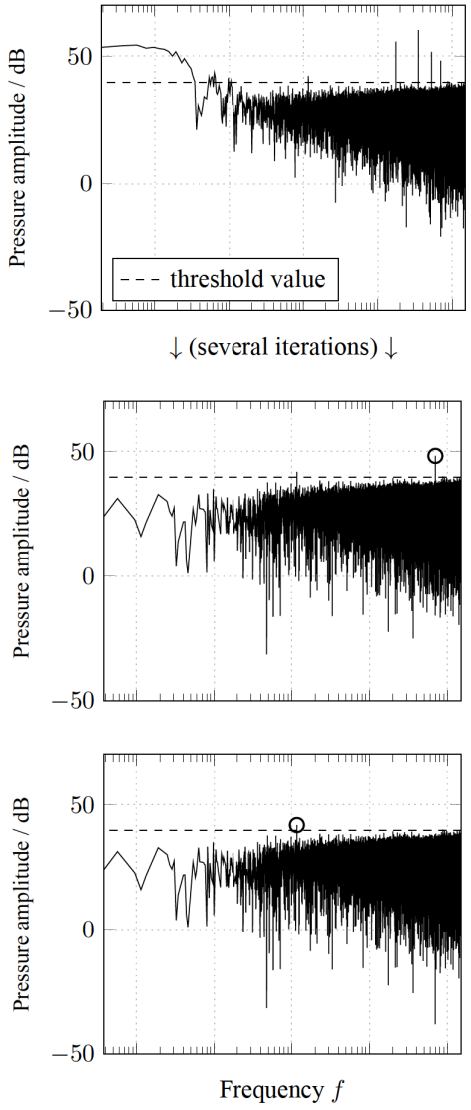

Figure 4: **Deconvolution iterations in the frequency domain**

Abort Criterion

A critical step of the algorithm is finding an appropriate threshold value to define the abort criterion in item 2. In the present study, two approaches were used: manual definition of a constant

threshold value and various multiples of the root mean square of the zero-centered signal spectrum

$$x_{thr} = \alpha \cdot \sqrt{\frac{\sum_{i=1}^{N} \left(\mathcal{F}_i \left(p(t) - \overline{p}(t)\right)\right)^2}{N}}, \tag{5}$$

where x_{thr} denotes the threshold value and α is an arbitrary factor. Other approaches are conceivable, such as an iterative re-definition of the threshold value in the deconvolution loop and definitions based on the relative power extracted from the original signal's autospectrum and may be implemented in further studies.

Comparison of Methods

The quantitative performance of both methods is compared, by using them to reduce the data of a generic signal. The signal is composed of a constant component, sine waves (frequencies similar to the rotational and blade passing frequencies of the measurement data presented below), and a triangular pulse (with a frequency half that of the assumed blade passing frequency) and superimposed with normally distributed random noise. The signal, its trace without noise and the PLEA as well as the deconvolution of the data are plotted in Fig. 5. The length of the deconvolved signal is identical to the original signal. The plotted trace represents approximately the same period as the PLEA, but is taken from the middle of the deconvolved signal.

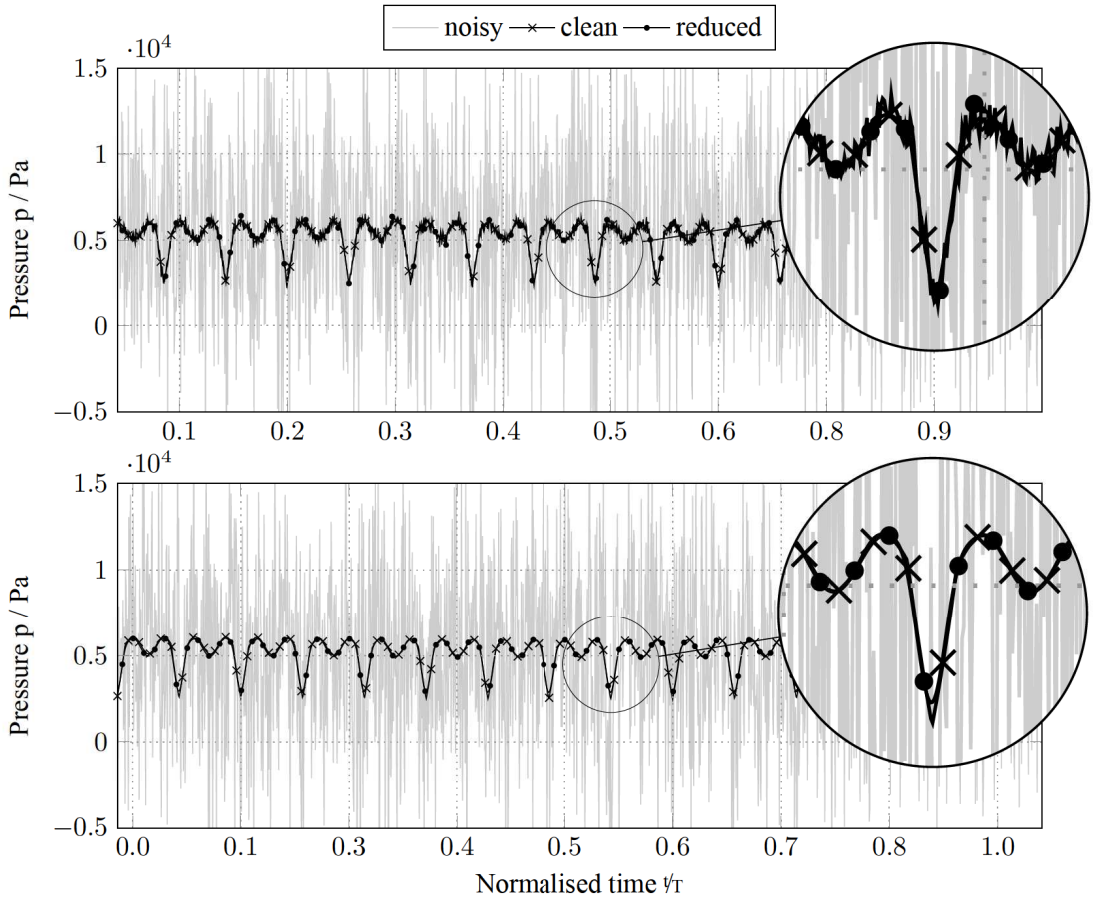

Figure 5: **Generic signal with superimposed, normally distributed noise reduced by PLEA (above) and deconvolution (below).**

It is clear, that the deconvolution method is capable of reassembling the deterministic signal in this generic case. To obtain a quantitative measure of the deviation of the reduced signals from the clean signal, the latter is subtracted from the former and the root mean square of the remainder is

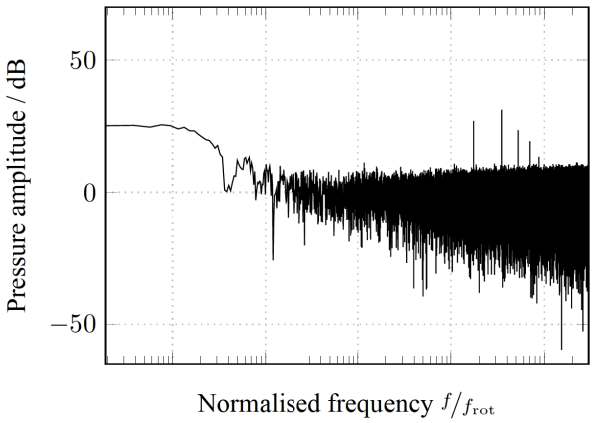

Figure 6: **FFT spectrum of the noisy generic signal.**

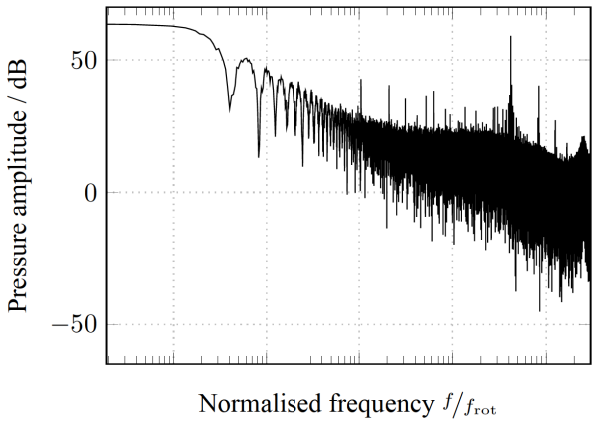

Figure 7: **FFT spectrum of a time-resolved signal recorded with the ZI45 probe.**

computed. The result is normalised by the root mean square of the noise (i.e. the difference between the noisy and the clean signal). The relative deviation of the PLEA is 4.15 %, while the deviation of the deconvolved signal is 1.52 % when evaluating the entire length of the signal, i.e. the same length as the original trace. The PLEA was computed from ensembles of 580 traces and the same data, though not phase-locked, was used for the deconvolution. Using larger ensembles of approximately 2900 traces reduces the PLEA deviation to less than 2 %.

Due to the limited resolution of numerical systems, adding the sinusoidal components of the deconvolution leads to "interference" effects. As a result, the deconvolved signal deviates strongly from the original signal near the beginning and end. When the relative deviation is computed for the deconvolved trace plotted in Fig. 5, it is reduced to 1.37 %. Increasing the signal length has the unfavourable side effect of intensifying this effect.

Another drawback of the proposed method in comparison to PLEA is a longer computation time. If implemented efficiently, the PLEA may need very little time even for large quantities of data. The computation time of the deconvolution, due to its iterative nature and use of Fourier transformations, exceeds that needed for PLEA—at times by far. However, the time needed is dependent on the nature of the signal as well as the selected threshold criterion. For the generic signal presented in Fig. 5, the reduction by deconvolution takes approximately ten times as long as the reduction by PLEA.

While a generic signal offers the opportunity to compare the reduced signals to a known "clean" signal, the superimposed noise does not mirror the conditions of actual measurement data. The spectrum of the generic signal (Fig. 6) illustrates the inadequacy of normally distributed white noise. The identification of periodic components is fairly trivial. Hence, the method is applied to measured data in the following section in order to determine its performance in realistic applications.

APPLICATION TO MEASURED DATA

The Fourier spectra of measured time-resolved data are generally more complex than the generic signal spectrum (cf. Fig. 6 and Fig. 7). Therefore the identification of deterministic components is not as straightforward. In order to demonstrate the applicability, as well as the limitations of the deconvolution method when used on measurement data, a set of time-resolved pressure measurements were recorded aft of the stage 7 rotor of the test turbine described above.

The probe can be calibrated to measure the three-dimensional flow vector, but any further calibration has been omitted to avoid any additional sources of uncertainty as the flow vector is not relevant in this case. The deterministic spectrum is expected to be dominated by wake structures at blade passing frequency with some influence of the rotational frequency. No periodic components with frequencies other than (sub-)multiples of the rotational frequencies are expected to have significant

influence. Hence, ensemble averaging and deconvolution are expected to yield similar results for the same data.

The data was recorded at 200 kS/s for 5 seconds using synchronised sampling of the four probe channels as well as one trigger signal. Though it is not a prerequisite for the deconvolution method, the trigger signal can be used to cut the reassembled signal into sections corresponding to approximately one revolution of the rotor. For direct comparison with PLEA results, the obtained sections are then phase-locked by interpolation.

Figure 8 shows the comparison of PLEA and deconvolved signal reassembly at various radial positions in the measurement plane. Different abort criteria have been used for the deconvolution algorithm, each based empirically on the signal type and its specific signal-to-noise ratio. The results were obtained using two predefined, constant abort criteria and one derived from the signal. The latter threshold corresponds to $5 \cdot \mathrm{RMS}\left(\mathcal{F}(p)(t)\right)$ in the case denoted *auto*. More than 500 revolutions were used to obtain the PLEA in all cases.

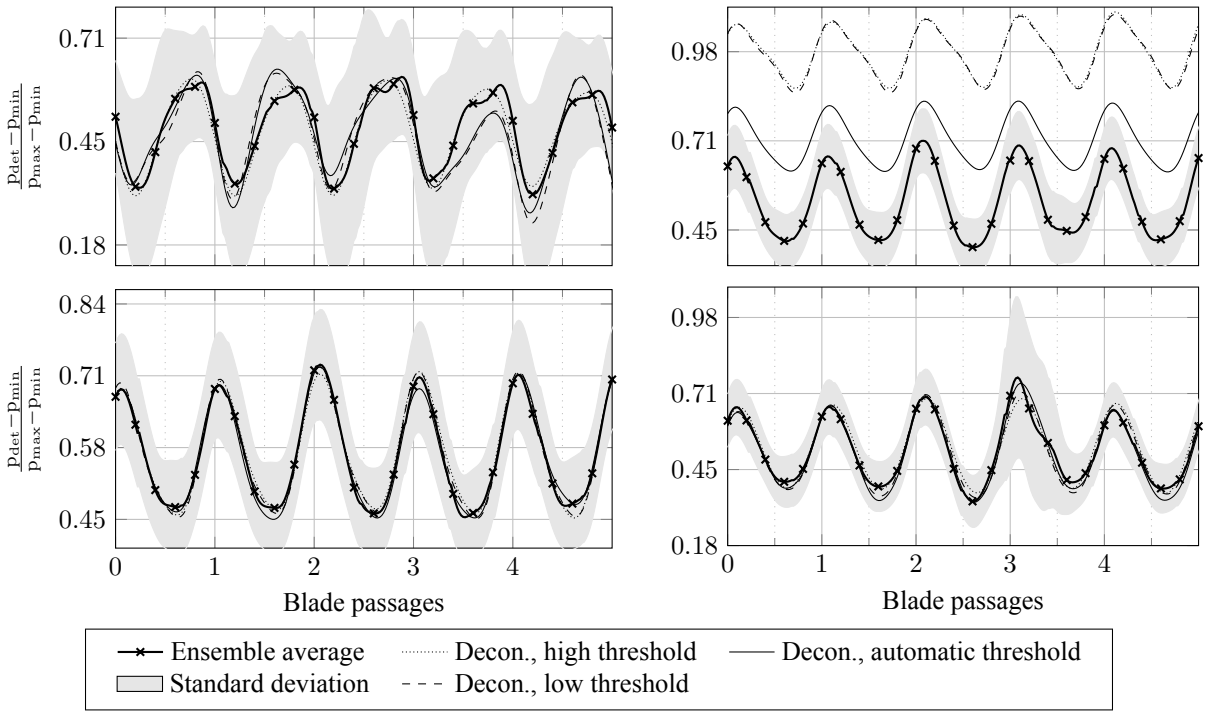

Figure 8: **Reduction of experimental data by PLEA and deconvolution at approximately 99 %, 65 %, 57.5 %, and 50 % (top left, bottom left, top right, bottom right) relative channel height.**

The four plots represent the reduced signals at approximately 50 %, 57.5 %, 65 %, and 99 % relative channel height. The reduction results of the sinusoidal signals at 50 % and 65 % correspond well with the PLEA result of the same data. The deconvolved signal at 99 % shows larger deviations from the PLEA. The result is, however, dependent on the abort criterion. The earliest abort of the deconvolution loop produces the best result in this case.

The grey area represents the magnitude of the stochastic signal components, i.e. the intermittent flow phenomena, turbulence, and noise. These values are based on the PLEA and represent the standard deviation of the noise computed from all phase-locked traces as a function of the rotor phase.

Contour plots of the entire radial traverse data reduced by deconvolution and PLEA are plotted in Fig. 9 and 10, respectively. The difference of both is plotted in Fig. 11; in most areas the difference is less than ± 10 %. The results indicate qualitative agreement of the two methods in respect to width and phase of the wakes as well as the absence of non-harmonic fluctuating components. The most notable difference is the reduced signal at approximately 57.5 % relative channel height (cf. Fig. 8,

top right). The error is a result of "interference" effects caused by limited numerical resolution of the frequency of signal components. Small differences of the frequencies of the generic signals g_i lead to errors in both the high and low frequency fluctuations. The seemingly constant error is most likely a result of a spurious low frequency fluctuation in the deconvolved signal.

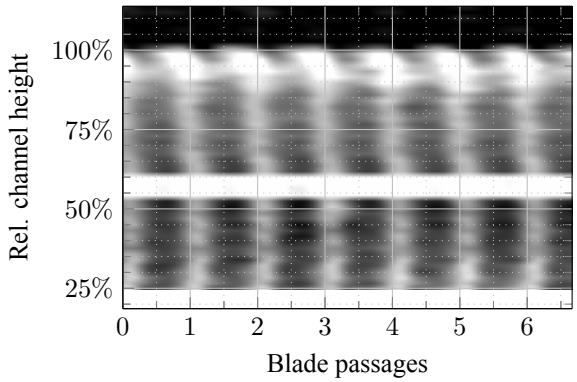

Figure 9: **Polar contour plot of deconvolved pressure signals at various radial positions.**

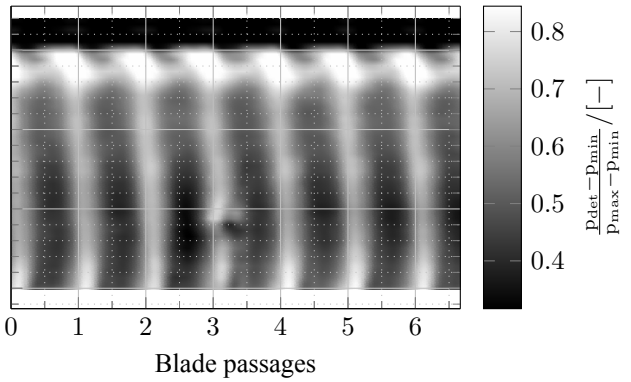

Figure 10: **Polar contour plot of the PLEA of the same data used for the deconvolution in Fig. 9.**

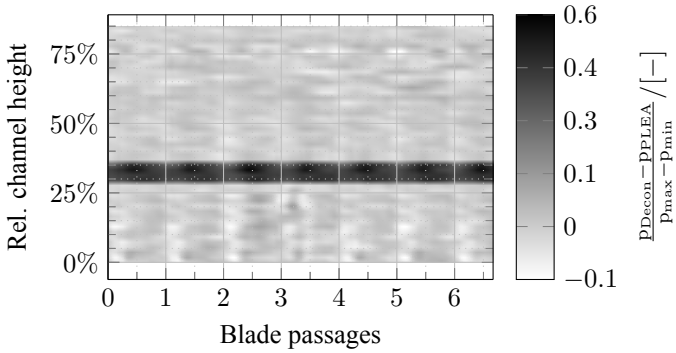

Figure 11: **Polar contour plot of the of the difference of the data in Fig. 9 and 10.**

CONCLUSIONS

The deconvolution data reduction method is proposed as an alternative to the phase-locked ensemble averaging method (PLEA) for the reduction of time-resolved turbomachinery measurements. The method makes the reassembly of deterministic (i.e. periodic) signal components from noisy raw signals possible without the necessity for a trigger signal.

Adequacy of the deconvolution method has been shown in comparison with PLEA results when applied to generic signals and pressure measurement data. For generic data sets with normally distributed noise, deconvolution proves to be more accurate than PLEA in the reassembly of the deterministic signal components. When applied to noisy measurement data, problems arise from the limited resolution of discrete numerical spectra as the reassembled signal components create interference-like effects when added. The problem of defining a threshold value for the abort criterion of the deconvolution iteration is approached by defining constant values and multiples of the root mean squares of the signal spectra. A potential source of errors lies in insufficient stability of the rotational speed. Its maximum influence can be quantified if the rotational frequency deviation is known. In most cases it can be expected to be small as high sampling rates entail short sampling times.

The deconvolution method is theoretically able to reassemble rotationally harmonic and, in contrast to PLEA, non-harmonic signal components as long as they are periodic. While the reassembly of rotationally harmonic components has been shown in comparison to PLEA and application to

measurement data, the feasibility of non-harmonic component reassembly has yet to be shown by application on appropriate measurement data in a next step. The method is well suited for the validation of PLEA results or the reduction of data recorded without synchronous trigger signals. It allows the quantification of target values such as the width of wake structures which cannot be easily derived from spectral information directly.

ACKNOWLEDGEMENTS

The authors would like to thank Siemens AG for their permission to publish the measurement data used for this study and AG Turbo for their support of the research project (0327718E).

REFERENCES

Binner, M. (2011): Experimentelle Untersuchung von Teil- und Schwachlastzuständen in Hochdruckdampfturbinen. Strömungsmechanik, Dr. Hut, Munich.

Binner, M. and Seume, J.R. (2014): *Flow Patterns in High Pressure Steam Turbines During Low-Load Operation*. In: J. Turbomach., vol. 136(6).

Bräunling, W.J.G. (2009): Flugzeugtriebwerke : Grundlagen, Aero-Thermodynamik, ideale und reale Kreisprozesse, thermische Turbomaschinen, Komponenten, Emissionen und Systeme. VDI-Buch, 3rd edn., Springer, Berlin.

Bubolz, T. (2005): Untersuchungen von randzonenkorrigierten Axialverdichterbeschaufelungen mit Strömungs-Meßsonden. Ph.D. thesis, Universität Hannover, Hanover.

Camp, T.R. and Shin, H.W. (1995): *Turbulence Intensity and Length Scale Measurements in Multistage Compressors*. In: J. Turbomach., vol. 117(1):pp. 38–46.

Gostelow, J.P. (1977): *A New Approach to the Experimental Study of Turbomachinery Flow Phenomena*. In: J. Eng. Power, vol. 99(1):pp. 97–105.

Herzog, N.; Binner, M.; Seume, J.R.; and Rothe, K. (2007): *Verification of Low-Flow Conditions in a Multistage Turbine*. In: Proceedings of the ASME Turbo Expo 2007, vol. 6, Part A, ASME, New York, pp. 563–574.

Högbom, J.A. (1974): *Aperture Synthesis with a Non-Regular Distribution of Interferometer Baselines*. In: Astron. Astrophys. Suppl., vol. 15:pp. 417–426.

Lengani, D.; Paradiso, B.; and Marn, A. (2012): *A Method for the Determination of Turbulence Intensity by Means of a Fast Response Pressure Probe and its Application in a LP Turbine*. In: J. Therm. Sci., vol. 21(1):pp. 21–31.

Mailach, R. (2010): Unsteady Flow in Turbomachinery. Habilitation, Technische Universität Dresden, Dresden.

Mailach, R.; Müller, L.; and Vogeler, K. (2004): *Rotor-Stator Interactions in a Four-Stage Low-Speed Axial Compressor–Part II: Unsteady Aerodynamic Forces of Rotor and Stator Blades*. In: J. Turbomach., vol. 126(4):pp. 519–526.

Meyer, R.X. (1958): *The Effect of Wakes on the Transient Pressure and Velocity Distributions in Turbomachines*. In: Trans. ASME, vol. 80(7):pp. 1544–1552.

Niehuis, R.; Lücking, P.; and Stubert, B. (1990): *Experimental and Numerical Study on Basic Phenomena of Secondary Flows in Turbines*. In: Secondary Flows in Turbomachines, vol. 469 of *AGARD Conf. Proc.*

Restemeier, M.S. (2012): Einfluss des Schaufelreihenabstands auf Strömung und Wirkungsgrade in einer subsonischen Axialturbine. 1st edn., Dr. Hut, Munich.

Rick, H. (2013): Gasturbinen und Flugantriebe : Grundlagen, Betriebsverhalten und Simulation. Springer Vieweg, Berlin.

Rieß, W. and Braun, M. (2003): Stationäres und instationäres Verhalten verschiedener Typen von Strömungs-Messsonden in instationärer Strömung. Strömungs-Messonden in instationärer Strömung. Abschlussbericht DFG-Normalverfahren Ri 375/13-1. Tech. Rep., Inst. f. Strömungsmaschinen, Universität Hannover, Hanover.

Ristic, D.; Lakshminarayana, B.; and Chu, S. (1999): *Three-Dimensional Flowfield Downstream of an Axial-Flow Turbine Rotor*. In: Journal of Propulsion and Power, vol. 15(2):pp. 334–344.

Schlichting, H. and Gersten, K. (2006): Grenzschicht-Theorie. 10th edn., Springer, Berlin.

Sharma, O.P.; Butler, T.L.; Joslyn, H.D.; and Dring, R.P. (1985): *Three-Dimensional Unsteady Flow in an Axial Flow Turbine*. In: Journal of Propulsion and Power, vol. 1(1):pp. 29–38.

Sieverding, C.H. (1985): *Recent Progress in the Understanding of Basic Aspects of Secondary Flows in Turbine Blade Passages*. In: Journal of Engineering for Gas Turbines and Power, vol. 107(2):pp. 248–257.